

Design Strategy of Highly Efficient Nonlinear Optical Orange-Colored Crystals with Two Electron-Withdrawing Groups

Seung-Jun Kim, Se-In Kim, Mojca Jazbinsek, Woojin Yoon, Hoseop Yun, Dongwook Kim, In Cheol Yu, Fabian Rotermund, and O-Pil Kwon*

A new class of highly efficient nonlinear optical organic salt crystals is reported. In nonlinear optics based on organic materials, it is well known that using two electron-withdrawing groups (EWGs) onto cationic electron acceptors instead of conventional one EWG remarkably enhances microscopic optical nonlinearity for chromophores. However, the corresponding organic crystals possessing enhanced large macroscopic optical nonlinearity have not been reported yet. Herein, a design strategy is proposed for obtaining highly efficient nonlinear optical crystals based on two EWGs in cationic electron acceptors. Introducing a phenolic electron donor, promoting a head-to-tail interionic assembly, along with a two-EWG N-pyrimidinyl pyridinium electron acceptor in cationic chromophores results in a preferred non-centrosymmetric, perfectly parallel alignment of chromophores in crystal. Newly designed OPR (4-(4-hydroxystyryl)-1-(pyrimidin-2-yl)pyridinium) crystals exhibit approximately two times larger effective first hyperpolarizability than that of analogous N-alkyl OHP (4-(4-hydroxystyryl)-1-methylpyridinium) crystals based on only one EWG. OPR crystals exhibit comparable second-order optical nonlinearity to benchmark red-colored DAST (4-(4-(dimethylamino)styryl)-1-methylpyridinium 4-methylbenzenesulfonate) crystals, but a significant blue-shifted absorption resulting in orange-color crystals. Therefore, phenolic organic salt crystals using two EWGs are highly promising materials for various nonlinear optical applications.


1. Introduction

Organic crystals exhibiting second-order optical nonlinearity enable strong interaction of electromagnetic waves and zero-frequency electric fields with matter. These interactions result in changes and modulation of the characteristics of electromagnetic waves such as frequency, phase, time delay, and amplitude. This nonlinear response of organic crystals can be applied for various nonlinear optical and electro-optic applications.^[1–10] In the past few decades, many studies on organic nonlinear optical crystals have been carried out to enhance their macroscopic second-order optical nonlinearity toward improving the nonlinear optical performance.^[10,11] However, enhancing the macroscopic optical nonlinearity of organic crystals is highly challenging. In polymeric systems, the required noncentrosymmetric molecular ordering of polar chromophores can be achieved with additional forces (e.g., a poling process using an electric field).^[7,12] In the crystalline state, however, such a non-centrosymmetric molecular ordering must

be achieved through self-assembly without additional external forces. Consequently, although chromophores themselves may

S.-J. Kim, S.-I. Kim, O.-P. Kwon
Department of Molecular Science and Technology
Ajou University
Suwon 443-749, Korea
E-mail: opilkwon@ajou.ac.kr

M. Jazbinsek
Institute of Computational Physics
Zurich University of Applied Sciences (ZHAW)
8401 Winterthur, Switzerland

 The ORCID identification number(s) for the author(s) of this article can be found under <https://doi.org/10.1002/adpr.202100350>.

© 2022 The Authors. Advanced Photonics Research published by Wiley-VCH GmbH. This is an open access article under the terms of the Creative Commons Attribution License, which permits use, distribution and reproduction in any medium, provided the original work is properly cited.

DOI: 10.1002/adpr.202100350

W. Yoon, H. Yun
Department of Chemistry & Department of Energy Systems Research
Ajou University
Suwon 443-749, Korea

D. Kim
Department of Chemistry
Kyonggi University
San 94-6, Iui-dong, Yeongtong-gu, Suwonsi, Gyeonggi 443-760, Korea

I. C. Yu, F. Rotermund
Department of Physics
Korea Advanced Institute of Science and Technology (KAIST)
Daejeon 34141, Korea

exhibit large microscopic optical nonlinearity, in many cases, they form centrosymmetric molecular self-assemblies in the crystalline state, leading to vanishing macroscopic second-order optical nonlinearity.

In this work, we report a new class of organic salt crystals having very large macroscopic second-order optical nonlinearity. To achieve a large macroscopic optical nonlinearity in the crystalline state, previous studies often employed chromophores with various cationic electron acceptors, such as those based on pyridinium, quinolinium, benzothiazolium, or indolinium cations, which are π -electron-deficient electron-withdrawing groups (EWGs).^[6,13–23] To date, many benchmark organic salt crystals that exhibit top-level macroscopic optical nonlinearity have been based on an EWG.^[6,13–21] For instance, in widely used N-alkyl-substituted cationic electron acceptors (e.g., N-alkyl pyridinium), an EWG (pyridinium group) is incorporated with a non-EWG (alkyl group). The alkyl group is an electron-donating group (EDG) without electron-withdrawing strength. Introducing two EWGs onto cationic chromophores instead of only one is known to significantly improve the molecular optical nonlinearity for chromophores. For example, the microscopic optical nonlinearities of a chromophore based on two EWGs, N-pyrimidinyl pyridinium, can be several times higher than those of chromophores based on one EWG, N-alkyl pyridinium.^[22–26] Note that the pyrimidinyl group is a π -electron-deficient heteroaryl EWG. However, the corresponding nonlinear optical salt crystals using two EWGs with large macroscopic second-order optical nonlinearity have not yet been realized. Only a few examples of crystals that unfortunately show centrosymmetric molecular ordering (or very small macroscopic optical nonlinearity) have been reported.

In this study, we realized the first, to the best of our knowledge, nonlinear optical salt crystals using two EWGs on cationic electron acceptors that exhibit state-of-the-art

macroscopic optical nonlinearity. In the newly designed OPR (4-(4-hydroxystyryl)-1-(pyrimidin-2-yl)pyridinium, **Figure 1**) crystals, we introduced a two-EWG N-pyrimidinyl pyridinium electron acceptor along with a phenolic electron donor that promotes a head-to-tail interionic assembly. OPR crystals exhibit a very large diagonal effective hyperpolarizability tensor element of about 200×10^{-30} esu. This is about two times larger than that of analogous N-alkyl crystals based on only one EWG. Compared to benchmark organic crystals, OPR crystals exhibit very interesting and distinguishable physical, optical, and material properties, such as the blue-shifted absorption and various crystal morphologies with either in-plane or out-of-plane polar axis depending on the counter anion. Therefore, introducing two EWGs on cationic electron acceptors along with a phenolic electron donor is a promising design strategy for obtaining highly efficient nonlinear optical organic salt crystals.

2. Results and Discussion

2.1. New Chromophores with Enhanced Microscopic Optical Nonlinearity

The chemical structures of the newly designed OPR-based salt crystals are presented in Figure 1a. For the OPR cationic chromophore, we introduced two EWGs onto the electron acceptor (π -electron-deficient heteroaryl N-pyrimidinyl group on pyridinium group) that is classified here as the EWG-on-EWG electron acceptor (Figure 1b). The widely used N-alkyl pyridinium electron acceptor^[6,13–21] is classified as the EDG-on-EWG electron acceptor. Consequently, OPR cationic chromophores based on two EWGs may result in large molecular optical nonlinearities.

We chose the phenolic electron donor for the OPR cationic chromophore, because this donor has previously shown a high

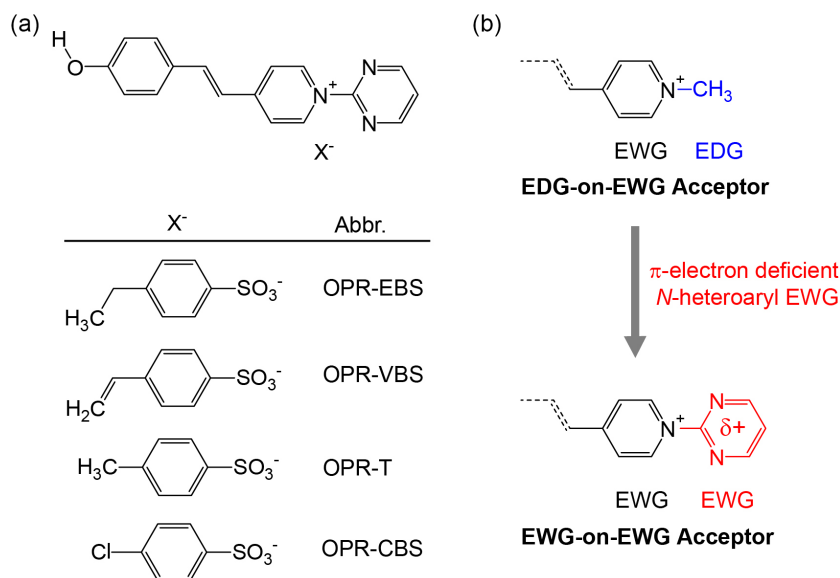


Figure 1. a) Newly designed nonlinear optical OPR crystals based on two electron-withdrawing groups (EWGs); N-pyrimidinyl and pyridinium groups. b) Enhancing molecular optical nonlinearity of OPR cationic chromophores by introducing two EWGs (EWG-on-EWG) onto electron acceptors instead of an EWG (EDG-on-EWG).

tendency to form non-Coulombic head-to-tail interionic assemblies with benzenesulfonate anions, which may be helpful for achieving noncentrosymmetric molecular ordering in the crystal-line state.^[6,16,17] As a counter ion, four benzenesulfonate anions, 4-ethylbenzenesulfonate (EBS), 4-vinylbenzenesulfonate (VBS), 4-methylbenzenesulfonate (T), and 4-chlorobenzenesulfonate (CBS) were employed.

To evaluate the microscopic optical nonlinearity of the OPR chromophore, quantum chemical calculations and nuclear magnetic resonance (NMR) measurements were performed. The first hyperpolarizability along the main charge-transfer direction, β_{\max} of the OPR cationic chromophore is calculated via the density functional theory calculations with B3LYP functional and 6-311 + G(d,p) basis sets.^[27,28] These results and other physical and crystallographic properties are listed in Table 1. For its calculated optimized structure (OPT), the N-pyrimidinyl OPR cation exhibits a very large microscopic optical nonlinearity; the first hyperpolarizability β_{\max} amounts to 183×10^{-30} esu. For experimental conformations (EXP) of OPR cations in the crystal-line state (i.e., conformations obtained from the X-ray structure analysis of single crystals), the calculated microscopic optical nonlinearity is similarly high. The first hyperpolarizability β_{\max} value of the OPR (EXP) cation in OPR-EBS, OPR-VBS, OPR-T, and OPR-CBS crystals is $191\text{--}204 \times 10^{-30}$ esu as listed in Table 1.

It is useful to recall that the first hyperpolarizability β_{\max} of N-alkyl analog OHP (4-(4-hydroxystyryl)-1-methylpyridinium) cation that has an EDG-on-EWG electron acceptor was 107 and 118×10^{-30} esu for OPT and EXP conformations, respectively, evaluated by equivalent density functional theory calculations.^[6] Note that N-alkyl OHP crystals show a highly efficient nonlinear optical response for difference frequency generation in the optical-to-THz frequency conversion process.^[6] The β_{\max} value of the OPR chromophores having an EWG-on-EWG electron acceptor shows a remarkable enhancement of about two times compared to OHP chromophores, considering the small structural difference between them; electron-donating N-alkyl substituent versus electron-withdrawing N-pyrimidinyl substituent on the electron acceptor. ¹H NMR measurements of the intermediates for these cationic chromophores also confirmed that N-pyrimidinyl pyridinium is more strongly electron-withdrawing than N-alkyl pyridinium. Figure 2

shows that the proton peak for the active methyl group on pyridinium (red star) appears at a higher chemical shift for the intermediate of the OPR cation (2.77 ppm) than for the intermediate of the OHP cation (2.59 ppm), reflecting the stronger electron-withdrawing character of the former. In addition, the pyridinium Ar-H peaks (blue and sky blue stars) also appear at higher chemical shifts for the intermediate of the OPR cation.

As listed in Table 1, the microscopic optical nonlinearity β_{\max} (OPT and EXP) of OPR cations ($183\text{--}204 \times 10^{-30}$ esu) is comparable to that of the current benchmark DAST (4-(4-(dimethylamino)styryl)-1-methylpyridinium 4-methylbenzenesulfonate)^[13] crystals ($159\text{--}194 \times 10^{-30}$ esu) that are obtained by nearly identical density functional theory calculations to the current study.^[28] Note that compared to the OPR chromophore, the DAS (4-(4-(dimethylamino)styryl)-1-methylpyridinium) chromophore in DAST possesses a largely different type of both the electron donor and the electron acceptor. While the DAS chromophore consists of the dimethylamino electron donor and an EDG-on-EWG electron acceptor (N-methyl pyridinium), the OPR chromophore consists of the hydroxyl electron donor and an EWG-on-EWG electron acceptor (N-pyrimidinyl pyridinium).

2.2. Large Macroscopic Optical Nonlinearity

All the OPR crystals, with different benzenesulfonate anions (EBS, VBS, T, and CBS), exhibit isomorphic crystal structures with space group symmetry *P1*, with one molecular pair (cation and anion) per unit cell. Figure 3a–d shows the overall molecular ordering features of the four OPR crystals. In these crystals, the OPR cationic chromophores exhibit perfectly parallel alignment. This alignment is attributed to linear head-to-tail cation-anion and cation-cation interactions of OPR cations (Figure 3e–h). Both the phenolic electron donor and the two-EWG N-pyrimidinyl pyridinium electron acceptor are strongly involved in the interionic interactions in crystals. The OPR cation possesses a very planar conformation (Figure 3e) and forms a linear head-to-tail cation-anion interaction based on the strong hydrogen bond between O—H(δ^+)...(δ^-)O—S groups (Figure 3f). In addition, OPR cations form a linear head-to-tail cation–cation interaction (Figure 3g). The details of interionic interactions with

Table 1. Summary of the physical and crystallographic properties of OPR, OHP, and DAST crystals.

| | OPR-EBS | OPR-VBS | OPR-T | OPR-CBS | OHP-CBS ^[6] | DAST ^[13,14,28] |
|---|---------------------|---------------------|---------------------|---------------------|------------------------|----------------------------|
| λ_{\max} in methanol [nm] | 443 | 443 | 443 | 443 | 390 | 475 |
| crystal color | orange | orange | orange | Orange | yellow | red |
| T_m [°C] | 289 | 318 | 306 | 320 | 270 | 256 |
| crystal system | triclinic <i>P1</i> | triclinic <i>P1</i> | triclinic <i>P1</i> | triclinic <i>P1</i> | triclinic <i>P1</i> | monoclinic <i>Cc</i> |
| β_{\max} (OPT) [10^{-30} esu] | 183 | 183 | 183 | 183 | 107 | 159 |
| β_{\max} (EXP) [10^{-30} esu] | 204 | 202 | 192 | 191 | 118 | 194 |
| θ_p [°] | 0 | 0 | 0 | 0 | 0 | 20 |
| order parameter $\cos^3\theta_p$ | 1.0 | 1.0 | 1.0 | 1.0 | 1.0 | 0.83 |
| largest diagonal β_{iii}^{eff} [10^{-30} esu] | 204 | 202 | 192 | 191 | 118 | 161 |
| largest off-diagonal β_{ijk}^{eff} [10^{-30} esu] | <4.0 | <4.0 | <4.0 | <4.0 | <3.0 | 21 |

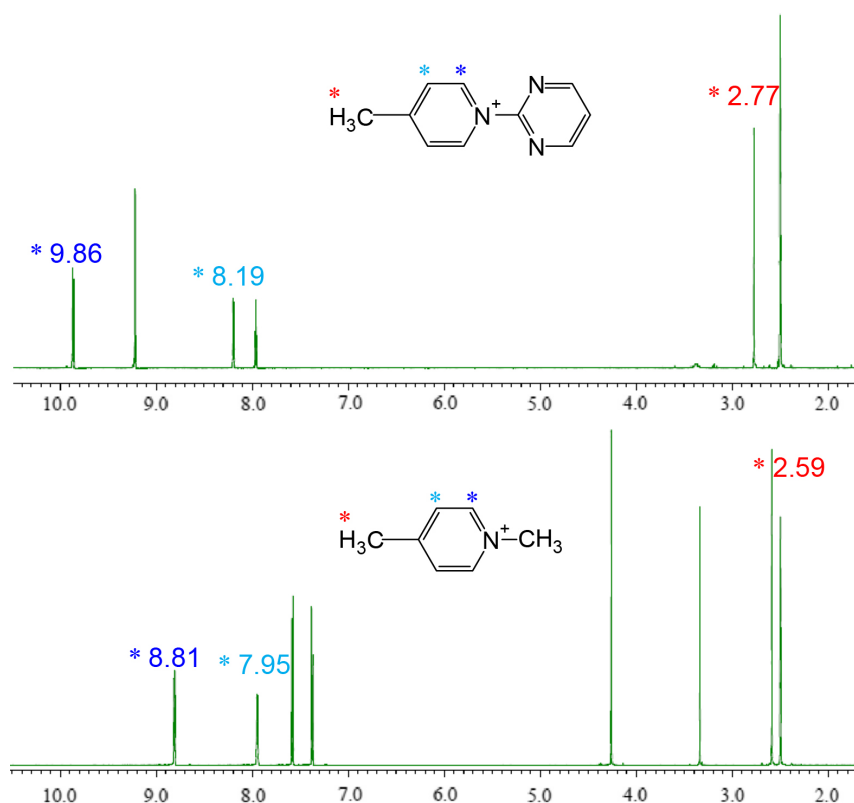


Figure 2. ^1H NMR spectra of intermediates in dimethyl sulfoxide- d_6 (DMSO- d_6): 4-methyl-1-(pyrimidin-2-yl)pyridin-1-ium chloride for N-pyrimidinyl OPR cationic chromophore and 1,4-dimethylpyridinium 4-chlorobenzenesulfonate for analogous N-alkyl chromophore.

Hirshfeld surface analysis^[29–31] are described in Supporting Information (Figure S1–S3, Supporting Information).

The polar axis for the OPR crystals and the direction of the first hyperpolarizability β_{max} of the OPR (EXP) cations are perfectly parallel because of the space group symmetry $P1$ as shown in Figure 3a–d. Consequently, the order parameter for each OPR crystal corresponds to the maximum value ($\cos^3\theta_p = 1.0$), where θ_p is the molecular-ordering angle (Table 1).^[11] The macroscopic optical nonlinearity of the OPR crystals is also very large; the diagonal component of the effective hyperpolarizability tensor β_{iii}^{eff} is equal to the β_{max} value of the corresponding OPR chromophore (EXP conformation) as listed in Table 1. These β_{iii}^{eff} values ($191\text{--}204 \times 10^{-30}$ esu) for OPR crystals with two EWGs are almost twice as large compared to those of the analogous N-alkyl OHP crystals with an EWG ($\beta_{iii}^{\text{eff}} = 118 \times 10^{-30}$ esu).^[6] Note that the index in the notation i refers to the direction along the polar axis of different crystals. In all OPR crystals, this direction is practically in the ab crystallographic plane (only about $5\text{--}6^\circ$ off this plane for all crystals) with the largest component along the crystallographic b axis (the polar axis is rotated by about $24\text{--}25^\circ$ from the crystallographic b or $-b$ axis in the ab plane for all crystals). Figure 3a–d shows the projection of the polar axis to the plane normal to the crystallographic a axis.

To evaluate the macroscopic optical nonlinearity of OPR crystals experimentally, powder second harmonic generation (SHG)

measurements^[32,33] were performed at various fundamental wavelengths as shown in Figure 4 (and Figure S4, Supporting Information). We can roughly distinguish two different regimes of the fundamental wavelengths: resonant fundamental wavelengths (<1600 nm) for which the second-harmonic wavelengths (<800 nm) are close to the electronic absorption band and non-resonant fundamental wavelengths (>1600 nm). At non-resonant fundamental wavelengths (1650, 1700, and 1800 nm), the average ratio of the SHG intensity of OPR-EBS and OPR-T powders relative to DAST powders is about 0.75 and 0.78, respectively (Figure 4). For OPR crystals, the largest off-diagonal component ($<4 \times 10^{-30}$ esu, Table 1) is practically negligible due to the perfectly parallel chromophore alignment. Therefore, the diagonal component of the macroscopic optical nonlinearity solely contributes to the SHG efficiency for OPR crystals. In contrast, for DAST crystals, the largest off-diagonal component of the effective hyperpolarizability tensor of 21×10^{-30} esu^[28] is not negligibly small and therefore contributes to the powder SHG efficiency. Consequently, these SHG results for the pump wavelengths above 1600 nm show that the diagonal optical nonlinearity (β_{iii}^{eff}) of OPR is comparable to that of DAST. From the aforementioned experimental and theoretical results, it is obvious that the diagonal macroscopic optical nonlinearity of OPR crystals is very large and comparable to that of DAST crystals and other various benchmark organic nonlinear optical crystals.^[11,34]

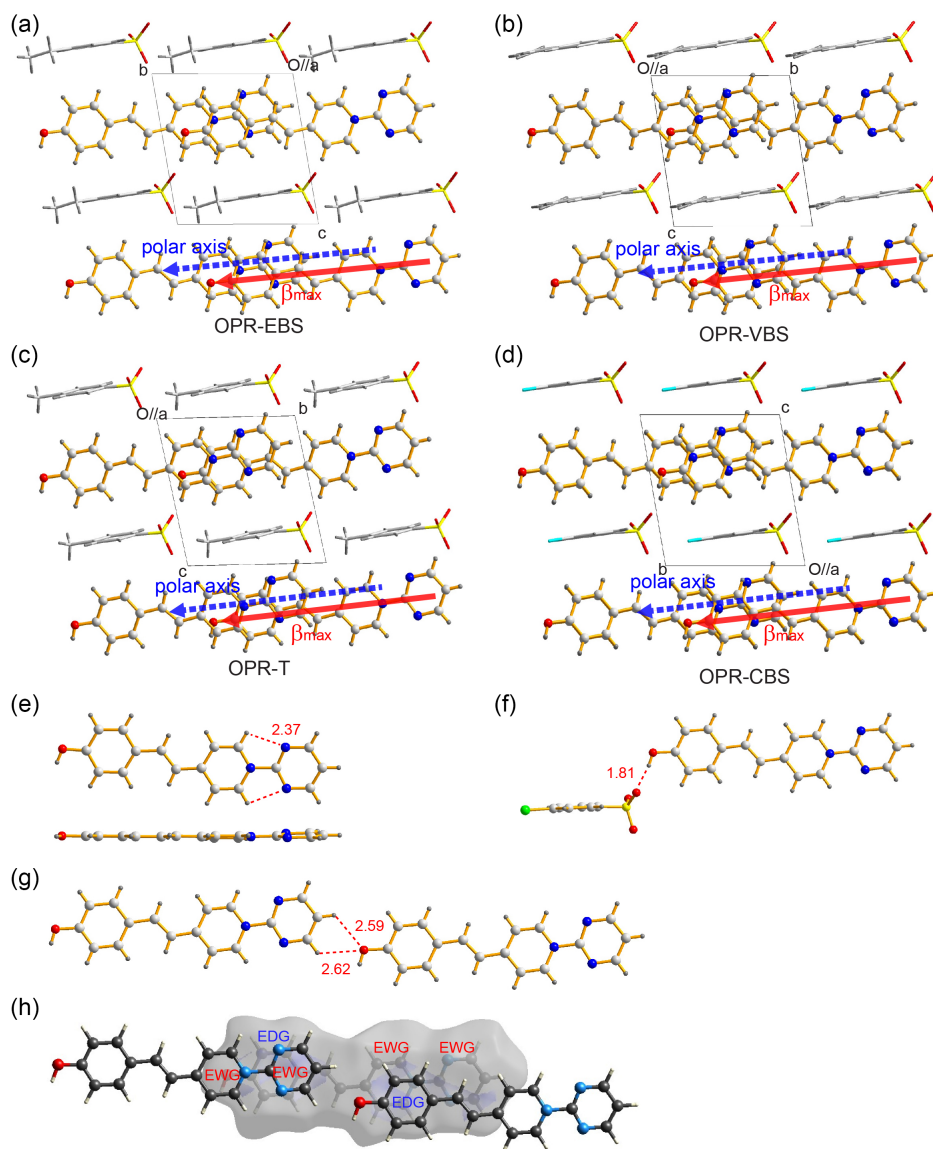


Figure 3. a–d) Molecular ordering features of OPR crystals projected along the crystallographic *a*-axis: a) OPR-EBS, b) OPR-VBS, c) OPR-T, and d) OPR-CBS. The solid and the dotted arrows present the direction of the first hyperpolarizability β_{\max} of the OPR (EXP) cation and the polar axis for the OPR crystals, respectively, projected to the displayed crystal plane. e–h) Representative non-Coulombic interionic interactions of OPR-based crystals (OPR-CBS): e) planar OPR cation: top-view and side-view, f) head-to-tail cation-anion interaction, g) head-to-tail cation-cation interactions, and h) stacking interactions between OPR cations, showing C...C atom contacts (blue region) of the Hirshfeld surface.

2.3. Crystalline Characteristics with Orange Color

In addition to the large diagonal macroscopic optical nonlinearity comparable to DAST crystals, all OPR crystals show a high thermal stability, which is very important for the long-term stability and operation of optical nonlinearity. As shown by the differential scanning calorimetry (DSC) and thermogravimetric analysis (TGA) in Figure S5, Supporting Information, all OPR crystals exhibit a very high melting temperature T_m ; 289, 318, 306, and 320 °C for OPR-EBS, OPR-VBS, OPR-T, and OPR-CBS, respectively. OPR crystals with alkyl substituent on anion (OPR-EBS and OPR-T) exhibit a 10–30 °C lower melting

temperature T_m than OPR crystals with non-alkyl substituent on anion (OPR-VBS, and OPR-CBS). Non-alkyl substituted OPR-VBS and OPR-CBS crystals exhibit an about 60 °C higher melting temperature T_m compared to DAST and its analogues (below 260 °C).^[14] In addition, OPR-CBS crystals exhibit an about 50 °C higher melting temperature T_m compared to OHP crystals with identical CBS anions (Table 1).^[6]

Figure 5 shows photographs of OPR-based single crystals grown in a mixture of methanol and acetonitrile (1:1 mol mol⁻¹) as described in Supporting Information. For nonlinear optical applications, one of the very important factors is the direction of the polar axis of as-grown single crystals, which determines

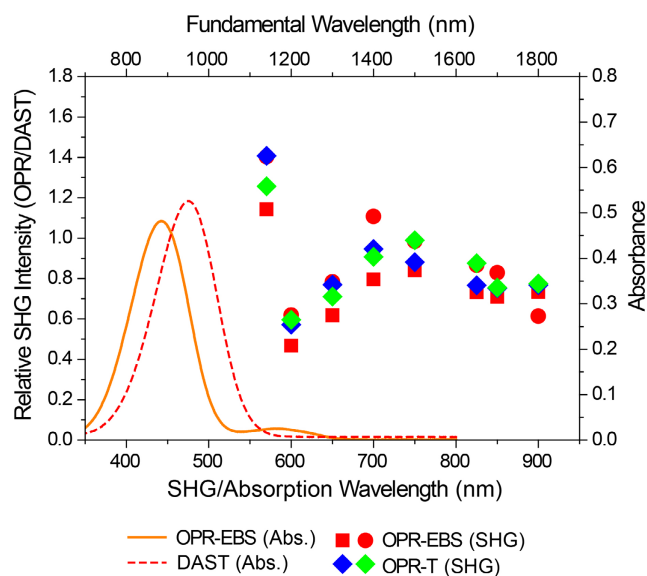


Figure 4. SHG intensity of OPR-EBS and OPR-T relative to that of DAST crystalline powders (left vertical scale) and absorption spectra (right vertical scale) of OPR-EBS and DAST in methanol (10^{-3} M).

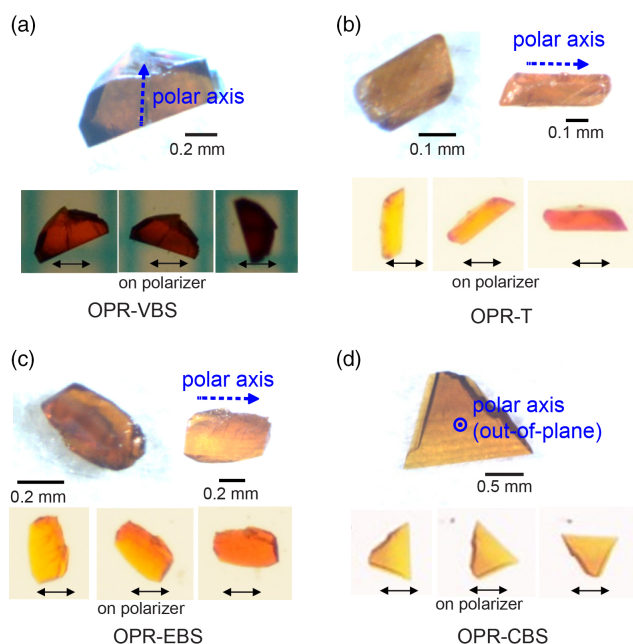


Figure 5. Photographs of as-grown OPR-based crystals: a) OPR-VBS, b) OPR-T, c) OPR-EBS, and d) OPR-CBS.

the optimal optical configuration for various applications. This is important because it is often very challenging to grow highly nonlinear optical organic crystals of size and quality that would allow subsequent cutting along any desired crystallographic plane. When as-grown OPR-VBS, OPR-T, and OPR-EBS crystals were rotated on a polarizer, their transparencies varied significantly (Figure 5a–c). This transparency variation allows locating the direction of the polar axis along the largest crystal facet, based

on the largest absorption expected along this axis. In contrast, the transparency of the OPR-CBS crystals did not vary significantly depending on the light polarization (Figure 5d). The X-ray structure analysis showed a perfectly parallel alignment of chromophores in all crystals, which predicts a very strong anisotropy of the optical properties for the light polarization along and perpendicular to the polar axis. The OPR-VBS, OPR-T, and OPR-EBS crystals, therefore, clearly present an in-plane polar axis or at least a significant projection of the polar axis existing along the largest plane of the as-grown crystals, similar to the most well-known benchmark organic nonlinear optical crystals.

In contrast, as-grown OPR-CBS crystals present an out-of-plane polar axis, i.e., perpendicular (or at least close to perpendicular) to the overall largest plane of the crystals. In as-grown, highly efficient nonlinear optical crystals with a very high order parameter, an out-of-plane polar axis is rarely observed.^[9] For example, as-grown DAST and its analogous crystals often exhibit a plate-like morphology with an in-plane polar axis.^[14,35] Therefore, in addition to the top-level macroscopic optical nonlinearity and high thermal stability, OPR crystals can be grown with polar axes that point in various directions, giving OPR derivatives a great potential for diverse nonlinear optical applications.

Interestingly, although OPR crystals exhibit a comparable diagonal macroscopic optical nonlinearity to that of DAST, the color of OPR crystals is significantly blue-shifted compared to the benchmark DAST and its analogous crystals.^[13,14] While DAST crystals appear red in transmission, OPR-based single crystals are orange as shown in Figure 5. Therefore, in OPR and DAST crystals, a different wavelength dependence of the linear and the nonlinear optical response is expected. The color of the crystals in the transmission is determined by the so-called transmission cutoff wavelength of crystals, λ_{cutoff} .^[36] In benchmark organic nonlinear optical crystals with a high order parameter ($\cos^3\theta > 0.8$), the cutoff wavelength λ_{cutoff} increases with the wavelength of maximum absorption of the constituting chromophores in solution, λ_{max} ; e.g., for yellow-colored OHP crystals ($\lambda_{\text{max}} = 390$ nm and $\lambda_{\text{cutoff}} \approx 490$ nm), orange-colored HMQ (2-(4-hydroxystyryl)-1-methylquinolinium) crystals ($\lambda_{\text{max}} = 439$ nm and $\lambda_{\text{cutoff}} \approx 595$ nm), and red-colored DAST crystals ($\lambda_{\text{max}} = 475$ nm and $\lambda_{\text{cutoff}} \approx 700$ nm).^[6,36,37] Even more generally in many nonlinear optical organic crystals, yellow, orange, and red-colored crystals roughly correspond to the wavelength of maximum absorption, λ_{max} , of the constituting chromophores in solution (<420 , 420–450, and >450 nm, respectively).^[6,38]

As shown in Figure 4, the absorption wavelength of OPR chromophores is significantly shorter than that of DAST; the wavelength of absorption maximum λ_{max} values in methanol are 443 and 475 nm for OPR-EBS and DAST, respectively. When large macroscopic optical nonlinearity is achieved, possessing the shorter absorption wavelength of OPR crystals is very beneficial for achieving different wavelength dependences of both linear and nonlinear optical characteristics, as well as the photochemical stability.^[6,34,39,40] For many nonlinear optical applications, it is essential to avoid the absorption at the pump and/or probe wavelengths used, while some may also prefer to match the wavelengths used with the absorption and rely on resonance effects.

OPR and DAST crystals are, therefore, expected to exhibit a remarkably different wavelength dependence of their nonlinear optical response. To investigate the wavelength dependence of the nonlinear optical response, powder SHG measurements are additionally performed in the resonant regime using pump wavelengths below 1600 nm (1140–1500 nm). As shown in Figure 4, the SHG intensity of OPR crystals relative to DAST crystals varies significantly in this region. When the fundamental wavelength decreases, the relative SHG intensity of OPR crystals first slowly increases, then rapidly decreases at the fundamental wavelengths of 1200–1300 nm (i.e., SHG wavelength of 600–650 nm), and finally rapidly increases at the fundamental wavelength of 1140 nm. This variation can be explained by the different absorption characteristics of these crystals (i.e., orange-colored OPR ($\lambda_{\text{max}} = 443$ nm) and red-colored DAST ($\lambda_{\text{max}} = 475$ nm)). At SHG wavelengths of 600–700 nm, the SHG intensity of DAST is enhanced by the resonance enhancement effect (see Figure S4, Supporting Information), which is stronger compared to OPR, for which these wavelengths are further away from the resonance. In contrast, at the SHG wavelength of 570 nm, both the resonance enhancement effect of OPR and stronger self-absorption of DAST contribute to a significant increase of the SHG efficiency of OPR compared to DAST. Note that this explanation is rather qualitative and does not consider an eventual contribution of exact phase matching, which also affects the results of the powder SHG efficiency. In contrast, the small phenolate absorption band of OPR chromophores at 584 nm in solution is not expected to affect the SHG efficiency of OPR crystals. This is because in the crystalline state, the phenolate absorption band at 584 nm may be negligible compared to the phenolic absorption band at 443 nm. The details are described in Supporting Information (see Figure S6, Supporting Information). This behavior is often observed in phenolic organic push–pull chromophores with a strong EWG.^[41]

It is obvious that orange-colored OPR crystals show a great potential for nonlinear optical applications. Compared to red-colored DAST crystals, while keeping the same level of the macroscopic second-order optical nonlinearity, OPR crystals offer different optimal application wavelengths based on different wavelength dependence of linear and nonlinear optical characteristics, high thermal stability, presenting either an in-plane or out-of-plane polar axis depending on the counter anion. For obtaining more precise quantitative optical and nonlinear optical properties of OPR crystals, additional experiments are required with the growth of high-quality single crystals with a larger lateral size reaching a few-mm scale that will be addressed in future work. In contrast, small nonlinear optical crystals (e.g., micro- and nano-crystals) with different natural morphologies may be interesting for various nanophotonic applications.^[42–46]

3. Conclusion

In summary, we have reported the first, to the best of our knowledge, highly efficient nonlinear optical crystals based on cationic electron acceptors using two EWGs. The newly designed phenolic N-pyrimidinyl pyridinium OPR crystals exhibit state-of-the-art macroscopic optical nonlinearity with a very large effective hyperpolarizability tensor component of about 200×10^{-30} esu, which

is about twice of the analogous N-alkyl crystals with only one EWG. In addition, compared to benchmark organic nonlinear optical crystals, OPR derivatives offer various crystal morphologies and different wavelength dependence of the linear and the nonlinear optical properties. Therefore, the OPR crystals are very attractive for diverse nonlinear optical and electro-optic applications. In addition, the molecular design approach in this work, introducing two EWGs on cationic electron acceptors along with a phenolic electron donor is highly useful strategy for achieving a non-centrosymmetric crystal structure with parallel chromophore orientation and subsequently a high second-order optical nonlinearity in the crystalline state.

4. Experimental Section

The details of the synthesis, crystal structure analysis, crystal growth, supramolecular interaction analysis, powder SHG measurements, thermal stability, and absorption characteristics are described in the Supporting Information (SI).

Supporting Information

Supporting Information is available from the Wiley Online Library or from the author.

Acknowledgements

S.-J.K. and S.-I.K. contributed equally to this work. This work has been supported by the National Research Foundation of Korea (NRF) funded by the Ministry of Science, ICT & Future Planning, Korea (No. 2021R1A2C1005012, 2021R1A5A6002853, 2019K1A3A1A14057973) and Swiss National Science Foundation (SNSF), Switzerland (No. IZKSZ2_188194).

Conflict of Interest

The authors declare no conflict of interest.

Data Availability Statement

Research data are not shared.

Keywords

chromophores, nonlinear optics, photonic materials

Received: November 16, 2021

Revised: February 6, 2022

Published online: March 8, 2022

- [1] A. Schliesser, N. Picqué, T. W. Hänsch, *Nat. Photonics* **2012**, 6, 440.
- [2] M. Tonouchi, *Nat. Photonics* **2007**, 1, 97.
- [3] S. van Cleuvenbergen, P. Kedziora, J. L. Fillaut, T. Verbiest, K. Clays, H. Akdas-Kilig, F. Camerel, *Angew. Chem., Int. Ed.* **2017**, 56, 9546.
- [4] W. Zhu, L. Zhu, L. Sun, Y. Zhen, H. Dong, Z. Wei, W. Hu, *Angew. Chem., Int. Ed.* **2016**, 55, 14023.
- [5] M. H. Shin, S. H. Lee, B. J. Kang, M. Jazbinsek, W. Yoon, H. Yun, F. Rotermund, O. P. Kwon, *Adv. Funct. Mater.* **2018**, 28, 1805257.

- [6] C. U. Jeong, B. J. Kang, S. H. Lee, S. C. Lee, W. T. Kim, M. Jazbinsek, W. J. Yoon, H. S. Yun, D. Kim, F. Rotermund, O. P. Kwon, *Adv. Funct. Mater.* **2018**, *28*, 1801143.
- [7] L. R. Dalton, P. A. Sullivan, D. H. Bale, *Chem. Rev.* **2010**, *110*, 25.
- [8] G. A. Valdivia-Berroeta, K. C. Kenny, E. W. Jackson, J. C. Bloxham, A. X. Wayment, D. J. Brock, S. J. Smith, J. A. Johnson, D. J. Michaelis, *J. Mater. Chem. C* **2020**, *8*, 11079.
- [9] J. Y. Choi, S. J. Lee, S. C. Lee, C. U. Jeong, M. Jazbinsek, H. Yun, B. J. Kang, F. Rotermund, O. P. Kwon, *J. Mater. Chem. C* **2017**, *5*, 12602.
- [10] S. Kannan, A. Sekar, K. Sivaperuman, *J. Mater. Chem. C* **2020**, *5*, 12602.
- [11] S. H. Lee, M. Jazbinsek, C. P. Hauri, O. P. Kwon, *CrystEngComm* **2016**, *18*, 7180.
- [12] Y. Enami, C. T. Derose, D. Mathine, C. Loychik, C. Greenlee, R. A. Norwood, T. D. Kim, J. Luo, Y. Tian, A. K.-Y. Jen, N. Peyghambarian, *Nat. photonics* **2007**, *1*, 180.
- [13] S. R. Marder, J. W. Perry, W. P. Schaefer, *Science* **1989**, *245*, 626.
- [14] Z. Yang, L. Mutter, M. Stillhart, B. Ruiz, S. Aravazhi, M. Jazbinsek, A. Schneider, V. Gramlich, P. Günter, *Adv. Funct. Mater.* **2007**, *17*, 2018.
- [15] G. A. Valdivia-Berroeta, L. K. Heki, E. A. McMurray, L. A. Foote, S. H. Nazari, L. Y. Serafin, S. J. Smith, D. J. Michaelis, J. A. Johnson, *Adv. Opt. Mater.* **2018**, *6*, 1800383.
- [16] P. J. Park, J. H. Jeong, M. Jazbinsek, S. B. Choi, I. H. Baek, J. T. Kim, F. Rotermund, H. Yun, Y. S. Lee, P. Günter, O. P. Kwon, *Adv. Funct. Mater.* **2012**, *22*, 200.
- [17] S. H. Lee, J. Lu, S. J. Lee, J. H. Han, C. U. Jeong, S. C. Lee, X. Li, M. Jazbinsek, W. Yoon, H. Yun, B. J. Kang, F. Rotermund, K. A. Nelson, O. P. Kwon, *Adv. Mater.* **2017**, *29*, 1701748.
- [18] J. Shi, F. Liang, Y. He, X. Zhang, Z. Lin, D. Xu, Z. Hu, J. Yao, Y. Wu, *Chem. Commun.* **2019**, *55*, 7950.
- [19] G. A. Valdivia-Berroeta, E. W. Jackson, K. C. Kenney, A. X. Wayment, I. C. Tangen, C. B. Bahr, S. J. Smith, D. J. Michaelis, J. A. Johnson, *Adv. Funct. Mater.* **2020**, *30*, 1904786.
- [20] J. Shi, Y. He, F. Liang, X. Zhang, D. Xu, J. Yao, G. Zhang, Z. Hu, J. Yao, Y. Wu, *J. Mater. Chem. C* **2020**, *8*, 4226.
- [21] H. Chen, Q. Ma, Y. Zhou, Z. Yang, M. Jazbinsek, Y. Bian, N. Ye, D. Wang, H. Cao, W. He, *Cryst. Growth Des.* **2015**, *15*, 5560.
- [22] B. J. Coe, J. A. Harris, I. Asselberghs, K. Clays, G. Olbrechts, A. Persoons, J. T. Hupp, R. C. Johnson, S. J. Coles, M. B. Hursthouse, K. Nakatani, *Adv. Funct. Mater.* **2002**, *12*, 110.
- [23] B. J. Coe, J. A. Harris, I. Asselberghs, K. Wostyn, K. Clays, A. Persoons, B. S. Bruntschwig, S. J. Coles, T. Gelbrich, M. E. Light, M. B. Hursthouse, K. Nakatani, *Adv. Funct. Mater.* **2003**, *13*, 347.
- [24] B. J. Coe, S. P. Foxon, E. C. Harper, J. A. Harris, M. Helliwell, J. Raftery, I. Asselberghs, K. Clays, E. Franz, B. S. Bruntschwig, A. G. Fitch, *Dyes Pigm.* **2009**, *82*, 171.
- [25] K. Clays, B. J. Coe, *Chem. Mater.* **2003**, *15*, 642.
- [26] B. J. Coe, D. Beljonne, H. Vogel, J. Garin, J. Orduna, *J. Phys. Chem. A* **2005**, *109*, 10052.
- [27] S. J. Kwon, O. P. Kwon, J. I. Seo, M. Jazbinsek, L. Mutter, V. Gramlich, Y. S. Lee, H. Yun, P. Günter, *J. Phys. Chem. C* **2008**, *112*, 7846.
- [28] P. J. Kim, J. H. Jeong, M. Jazbinsek, S. J. Kwon, H. Yun, J. T. Kim, Y. S. Lee, I. H. Baek, F. Rotermund, P. Günter, O. P. Kwon, *CrystEngComm* **2011**, *13*, 444.
- [29] M. A. Spackman, D. Jayatilaka, *Cryst. Eng. Commun.* **2009**, *11*, 19.
- [30] J. J. McKinnon, D. Jayatilaka, M. A. Spackman, *Chem. Commun.* **2007**, 3814.
- [31] M. A. Spackman, J. J. McKinnon, *CrystEngComm* **2002**, *4*, 378.
- [32] S. K. Kurtz, T. T. Perry, *J. Appl. Phys.* **1968**, *39*, 3798.
- [33] I. Aramburu, J. Ortega, C. L. Folcia, J. Etxebarria, *Appl. Phys. Lett.* **2014**, *104*, 071107.
- [34] S. J. Kim, B. J. Kang, U. Puc, W. T. Kim, M. Jazbinsek, F. Rotermund, O. P. Kwon, *Adv. Opt. Mater.* **2021**, 2101019.
- [35] B. Ruiz, M. Jazbinsek, P. Günter, *Cryst. Growth Des.* **2008**, *8*, 4173.
- [36] F. Pan, M. S. Wong, C. Bosshard, P. Günter, *Adv. Mater.* **1996**, *8*, 592.
- [37] J. H. Jeong, B. J. Kang, J. S. Kim, M. Jazbinsek, S. H. Lee, S. C. Lee, I. H. Baek, H. Yun, J. Kim, Y. S. Lee, J. H. Lee, J. H. Kim, F. Rotermund, O. P. Kwon, *Sci. Rep.* **2013**, *3*, 3200.
- [38] C. Bosshard, M. Bösch, I. Liakatas, M. Jäger, P. Günter, *Nonlinear Optical Effects and Materials*, Springer Verlag, Berlin **2000**, Chap. 3.
- [39] Y. J. Cheng, J. Luo, S. Huang, X. Zhou, Z. Shi, T. D. Kim, D. H. Bale, S. Takahashi, A. Yick, B. M. Polishak, S. H. Jang, L. R. Dalton, P. J. Reid, W. H. Steier, A. K. Y. Jen, *Chem. Mater.* **2008**, *20*, 5047.
- [40] D. Rezzonico, S. J. Kwon, H. Figi, O. P. Kwon, M. Jazbinsek, P. Günter, *J. Chem. Phys.* **2008**, *128*, 124713.
- [41] M. H. Shin, W. T. Kim, S. I. Kim, S. J. Kim, I. C. Yu, S. W. Kim, M. Jazbinsek, W. Yoon, H. Yun, F. Rotermund, O. P. Kwon, *Adv. Sci.* **2020**, *7*, 2001738.
- [42] Y. Kaneko, S. Shimada, T. Fukuda, T. Kimura, H. Yokoi, H. Matsuda, T. Onodera, H. Kasai, S. Okada, H. Oikawa, H. Nakanishi, *Adv. Mater.* **2005**, *17*, 160.
- [43] M. L. Zheng, K. Fujita, W. Q. Chen, X. M. Duan, S. Kawata, *J. Phys. Chem. C* **2011**, *115*, 8988.
- [44] T. Tian, B. Cai, O. Sugihara, *Nanoscale* **2016**, *8*, 18882.
- [45] M. L. Zheng, W. Q. Chen, K. Fujita, X. M. Duan, S. Kawata, *Nanoscale* **2010**, *2*, 913.
- [46] R. Macchi, E. Cariati, D. Marinotto, D. Roberto, E. Tordin, R. Ugo, R. Bozio, M. Cozzuol, D. Pedron, G. Mattei, *J. Mater. Chem.* **2010**, *20*, 1885.